Thermal Ablation Induces Transitory Metastatic Growth by Means of the STAT3/c-Met Molecular Pathway in an Intrahepatic Colorectal Cancer Mouse Model

Haixing Liao, PhD • Muneeb Ahmed, MD • Aurelia Markezana, MSc • Guohua Zeng, MD, PhD •
Matthias Stechele, MD • Eithan Galun, MD, PhD • S. Nahum Goldberg, MD

From the Goldyne Savad Institute of Gene Therapy (H.L., A.M., M.S., E.G., S.N.G.) and Department of Radiology (S.N.G.), Hadassah Hebrew University Hospital, Jerusalem, Israel; First Affiliated Hospital of Guangzhou Medical University, No. 151 Yanjiang Xi Road, Yuexiu District, Guangzhou, Guangdong 510120, China (H.L., G.Z.); Laboratory for Minimally Invasive Tumor Therapies, Department of Radiology, Beth Israel Deaconess Medical Center, Harvard Medical School, Boston, Mass (M.A., S.N.G.); and Department of Radiology, Ludwig-Maximilians-University Hospital Munich, Munich, Germany (M.S.). Received May 5, 2019; revision requested July 3; final revision received October 7; accepted October 22. **Address correspondence to** H.L. (e-mail: *bluedad@163.com*).

Conflicts of interest are listed at the end of this article.

See also the editorial by Nikolic in this issue.

Background: Systemic protumorigenic effects have been noted after radiofrequency ablation (RFA) of normal liver and have been linked to an interleukin 6/signal transducer and activator of transcription 3 (STAT3)/hepatocyte growth factor (HGF)/tyrosine-protein kinase Met (c-Met)/vascular endothelial growth factor (VEGF) cytokinetic pathway.

Purpose: To elucidate kinetics of RFA protumorigenic effects on intrahepatic metastatic implantation and growth and determine potential molecular targets for pharmacologic suppression of these effects.

Materials and Methods: An intrahepatic metastasis model was established by implanting CT26 and MC38 tumor cells into 216 7–8-week-old male Balb/C and C57BL6 mice, respectively, by means of splenic injection. Between June 2017 and March 2019, mice underwent tumor injection, followed 24 hours later by either standardized RFA (70°C ± 1, 5 minutes, 1-cm tip) or a sham procedure (needle placement without heating) (12 animals per arm, $n = 48$). Next, RFA or sham procedures were performed, followed by splenic tumor cell injection at 1 day, 3 days, or 7 days later (six animals per arm, $n = 72$). Finally, PHA-665752 and S3I-201 were used to block c-Met or STAT3, respectively, prior to either RFA or sham treatment (six animals per arm, $n = 96$). Livers were harvested at 14 days for CT26 and 21days for MC38 for tumor quantification. Ki-67 and CD34 immunohistochemistry measured proliferative indexes and microvascular density, respectively. Data were compared with analysis of variance and the two-tailed Student t test.

Results: RFA performed after tumor cell injection induced increased metastatic tumor number ($103 ± 45$ vs $52 ± 44$ [CT26], $P = .009$ and $87 ± 51$ vs $39 ± 20$ [MC38], $P = .007$), cellular proliferation ($P < .001$ for both), and intratumoral neovascularization ($P < .001$ for both), compared with the sham procedure. Tumor cell injection performed 1 day and 3 days after RFA also increased these indexes ($P < .05$), while no difference was demonstrated for cell injection 7 days after RFA ($P > .05$). Adjuvant c-Met or STAT3 inhibition reduced intrahepatic metastatic parameters after RFA to baseline ($P < .03$), equivalent to the sham group ($P > .05$).

Conclusion: Radiofrequency ablation of normal liver promotes intrahepatic metastatic implantation and increased growth over a short-lived (1–3 days) temporal window in animal models. This phenomenon can be potentially neutralized with specific inhibition of pathways including hepatocyte growth factor/tyrosine-protein kinase Met and signal transducer and activator of transcription 3.

©RSNA, 2019

Online supplemental material is available for this article.

Radiofrequency ablation (RFA) guided by medical imaging is now commonly used to treat a wide range of focal primary and metastatic tumors in solid organs, primarily the liver (1,2). The growing adoption and clinical implementation of this technique can be attributed to its minimal invasiveness, low morbidity, and cost efficiency (3). Thus, hepatic RFA has been adopted in consensus guidelines as a first-line therapy for primary cancer (eg, hepatocellular carcinoma) (4) and as a second-line therapy for metastatic tumors such as colorectal cancer (5,6).

Despite various advantages, treatment efficacy remains challenging in some patient populations. This includes achieving complete ablation of tumors larger than 3 cm (1,2), where studies have suggested that RFA may be associated with higher tumor recurrence rates (7), in part due to the difficulty in achieving a periablational margin of more than 5 mm, which is associated with better clinical outcomes (8,9). Moreover, there is a growing amount of laboratory data supporting the contention that thermal ablation of normal liver required to achieve sufficient margins can increase

Abbreviations

c-Met = tyrosine-protein kinase Met, HGF = hepatocyte growth factor, HPF = high-power field, IL-6 = interleukin 6, PHA = c-Met inhibitor, RFA = radiofrequency ablation, S3I = STAT3 inhibitor, STAT3 = signal transducer and activator of transcription 3, VEGF = vascular endothelial growth factor

Summary

Radiofrequency ablation of normal liver promoted growth of microscopic metastases and implantation of tumor cells from splenic injection in murine models of colorectal cancer; this transitory effect lasted less than 1 week and can be suppressed by inhibiting hepatocyte growth factor/tyrosine-protein kinase Met or signal transducer and activator of transcription 3.

Key Results

- In an animal model, radiofrequency ablation induced greater metastatic tumor number versus sham procedure (103 vs 52 tumors for CT26 tumor cells, *P* = .009; 87 vs 39 for MC38 tumor cells; *P* = .007, respectively).

- Similarly, cellular proliferation and intratumoral neovascularization were greater for radiofrequency abalation versus the sham procedure (*P* < .001 for both).

- Interleukin 6/hepatocyte growth factor/tyrosine-protein kinase Met and signal transducer and activator of transcription 3/vascular endothelial growth factor receptor inhibition reduced protumorigenic effects of radiofrequency ablation.

the production and excretion of protumorigenic growth factors (10–12). These include interleukin 6 (IL-6), hepatocyte growth factor (HGF)/tyrosine-protein kinase Met (c-Met), and vascular endothelial growth factor (VEGF), which have been shown to increase local, serologic, and intratumoral cytokine, growth factor, and signal transducer and activator of transcription 3 (STAT3) transcription factor mediator activation, with associated increased cellular proliferation and angiogenesis (13–16).

Although the effect of RFA on increasing tumor growth of previously implanted tumors has been demonstrated (17–19), its influence on tumor implantation and engraftment is still unknown. Such tumor cell dissemination is believed to be a primary obligate condition for hematologic metastatic spread in solid tumors such as colorectal cancer (20,21). Moreover, the presence of circulating tumor cells in patients with cancer is well documented in numerous types of malignancies (21) and has been seen after liver surgery (11) and RFA of both the lung and liver (22,23). Although knowing precisely when protumorigenic effects are most active is critical for designing rational adjuvant therapeutic strategies to eliminate this effect, the kinetics of ablation-induced tumorigenesis on these processes is poorly defined. Accordingly, here we sought to answer these questions by determining *(a)* whether RFA has the potential to accelerate growth of intrahepatic metastasis in mice models of disseminated colorectal cancer; *(b)* the kinetics and the temporal window of this process (ie, identifying the times at which RFA influences metastatic seeding and growth); and *(c)* the extent that pharmacologically targeting known key cytokine mediators of HGF/c-Met/STAT3 can suppress RFA-induced stimulation of progressive metastases in these metastatic colorectal cancer models.

Materials and Methods

Animal experiments were performed from June 2017 to March 2019 according to a protocol approved by the Hadassah Hebrew University Medical Center Institutional Animal Care Committee. An Association for Assessment and Accreditation of Laboratory Animal Care International certificate has been granted to this facility.

Overview of Experimental Design

We used a total of 216 mice. In all experiments, we performed diffuse intrahepatic tumor cell implantation via portal venous delivery using direct intrasplenic injection. We injected two c-Met–positive murine colorectal cancer cell lines, CT26 and MC38, in syngeneic mouse strains, 7–8-week-old male Balb/C and C57BL6 mice, respectively. We conducted this study in several stages.

In the first phase, we assessed the effect of local hepatic thermal ablation on the growth of diffuse micrometastatic implants. First, we performed intrasplenic tumor cell injection, followed 24 hours later by either standardized hepatic RFA (exploratory laparotomy, left hepatic lobe RFA for 5 minutes titrated to 70°C) or sham procedure (needle placement only) (*n* = 12 per arm times two treatment arms times two models; total *n* = 48). Mice were killed at 14 days after RFA (for CT26-Balb/C mice) and at 21 days (for MC38-C57BL6 mice) (based on tumor growth kinetics). We harvested the whole liver to assess tumor load, proliferative indexes, and microvascular density.

In the second phase, to determine the effect of hepatic RFA on implantation of tumor cells circulating in the portal venous system (ie, mimicking a metastatic tumor shower), we first performed standardized RFA or sham procedure, followed by intrasplenic tumor cell injection at 1 day , 3 days, or 7 days later, using both tumor models (*n* = six per arm times two arms times two models times three injection time points; total *n* = 72 mice). As in the prior experiment, mice were killed at 14 or 21 days after implantation, and we assessed similar outcome measures.

In the third phase, we evaluated the role of blocking one of the key mechanistic pathways underlying postablation tumor stimulation, IL-6/HGF/c-Met/STAT3/VEGF, through the adjuvant use of either a c-Met receptor blocker (PHA-665752; Sigma-Aldrich, St Louis, Mo [0.83 gm/kg]) (12,13) or STAT3 inhibitor (S3I-201; Sigma-Aldrich [10 mg/kg]) (15). We injected a corresponding volume of saline into the control group (PHA, *n* = 12; saline, *n* = 12 in each arm for both mouse models). Mice in each arm were randomly allocated to undergo either standard RFA (*n* = 6) or a sham procedure (*n* = 6) 24 hours after intrasplenic tumor cell injection and 2 hours after intraperitoneal injection of PHA. Similarly, we administered the STAT3 inhibitor S3I-201 (Sigma-Aldrich; 10 mg/kg) to block this key transcription factor (S3I, *n* = 12; saline, *n* = 12 for each arm of both models), followed by either RFA (*n* = 6) or sham treatment (*n* = 6). Mice were killed 14 or 21 days after RFA.

Techniques regarding the animal models used, application of standardized RFA protocols, and preparation of pharmacologic inhibitors have been previously described (12,13,15–17), and detailed information can be found in Appendix E1 (online).
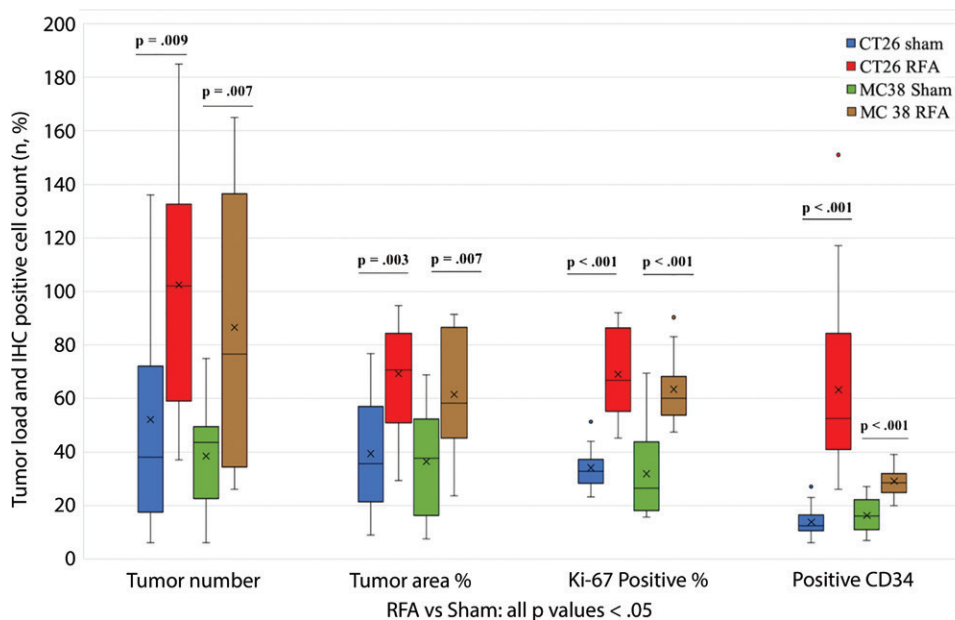
Figure 1: Box-whisker plot shows summary of the effect of tumorigenesis induced by radiofrequency ablation (RFA) in metastatic colorectal mouse tumor models. Comparisons of tumor load and number of Ki-67– and CD34-positive cells between RFA and sham procedures are shown. Tumor number and tumor area ratio in the mice livers that underwent RFA were significantly greater than those in mice that underwent a sham procedure. Likewise, the tumors identified in the RFA group had greater proliferative indexes and increased neovascularization than their littermates in the sham group. $P < .05$ for all comparisons of RFA versus sham procedure. IHC = immunohistochemistry.

Tissue Retrieval

After euthanasia, we excised the livers as one unit and photographed them in toto on both the ventral and dorsal surfaces. Thereafter, we transected the livers to include half of the coagulation zone including the periablational rim, tumor burden, and normal parenchyma in each specimen. We fixed samples in 10% formalin overnight at 4°C, embedded in paraffin, and sliced at a thickness of 5 μm.

Histologic Examination

We stained the tissues with hematoxylin-eosin for gross pathologic examination. We used specific immunohistochemical staining to quantitate the extent of cellular proliferation using a nuclear stain Ki-67 antibody (Thermo Fisher Scientific, Waltham, Mass; dilution 1:500) and microvascular density by staining the epithelial cytoplasm of intratumoral neovasculature with CD34 antibody (Bio-Rad, Hercules, Calif; dilution 1:100). Using optical microscopy (Micromaster I; Fisher Scientific, Pittsburgh, Pa) and software (Micron Imaging; Westover Scientific, Mill Creek, Wash), we imaged and analyzed the specimen slides. We analyzed five random fields under high-power magnification (×40) for a minimum of three specimens for each parameter and performed scoring in a blinded fashion to remove observer bias. For Ki-67, we calculated the percentage of positive cells (a ratio of stained and unstained cells) for each field and averaged for each specimen. Staining for CD34 and quantification of microvascular density was performed as previously described (13,16). As an additional control, to ensure uniformity of staining, immunohistochemistry was performed with all relevant comparison slides stained at the same time whenever direct comparisons were made.

Statistical Analysis

We assessed tumor load using two end points. First, we quantified the total number of visible tumors in each liver and categorized as being either less than or greater than 3 mm in diameter, as previously described (16). Additionally, to account for potential variations in tumor size, we calculated a "tumor ratio" as the percentage of tumor area to the entire liver for each mouse. Tumor surface area was measured in pixels by tracing all the tumor borders and the whole liver surface with image processing software (ImageJ, version 1.52a, *http://imagej. nih.gov/ij/download.html*, National Institutes of Health and the Laboratory for Optical and Computational Instrumentation, University of Wisconsin, Madison, Wis) for both the ventral and dorsal sides of the liver. For immunohistochemistry, the interpretation was performed by three individuals independently, with a consensus review performed whenever discrepancy was noted. Statistical significance of each end point for experimental phase and tumor type was evaluated by using pairwise *t* tests (Excel; Microsoft, Redmond, Wash), with *P* values adjusted by using a multiple comparison correction including the Benjamini-Hochberg procedure to account and correct for family-wise error rates (online calculator: *alexandercoppock.com*). Adjusted *P* values are reported and were considered significant if $P < .05$.

Results

Focal Hepatic RFA Stimulates Implantation and Intrahepatic Metastatic Growth

All animals survived cellular implantation, the hepatic ablation procedure, and the scheduled follow-up to the completion of the experiment. For both CT26 and MC38, the tumor load in mice that underwent hepatic RFA was greater than that in mice that underwent the sham procedure (CT26: 103 ± 45 vs 52 ± 44, *P* = .009; MC38: 87 ± 51 vs 39 ± 20, *P* = .007; RFA vs sham, respectively) (Figs 1, 2). Likewise, the tumor area ratio was greater for RFA than for sham (CT26: 69% ± 20 vs 39% ± 22, *P* = .003; MC38: 62% ± 22, vs 36% ± 20, *P* = .007) (Table 1, Fig 2). Tumors were distributed throughout all lobes of the liver, and given the extensive tumor burden, qualitatively no difference was noted for tumor distribution. Moreover, the tumors identified in the RFA group had greater proliferative indexes and increased neovascularization than those
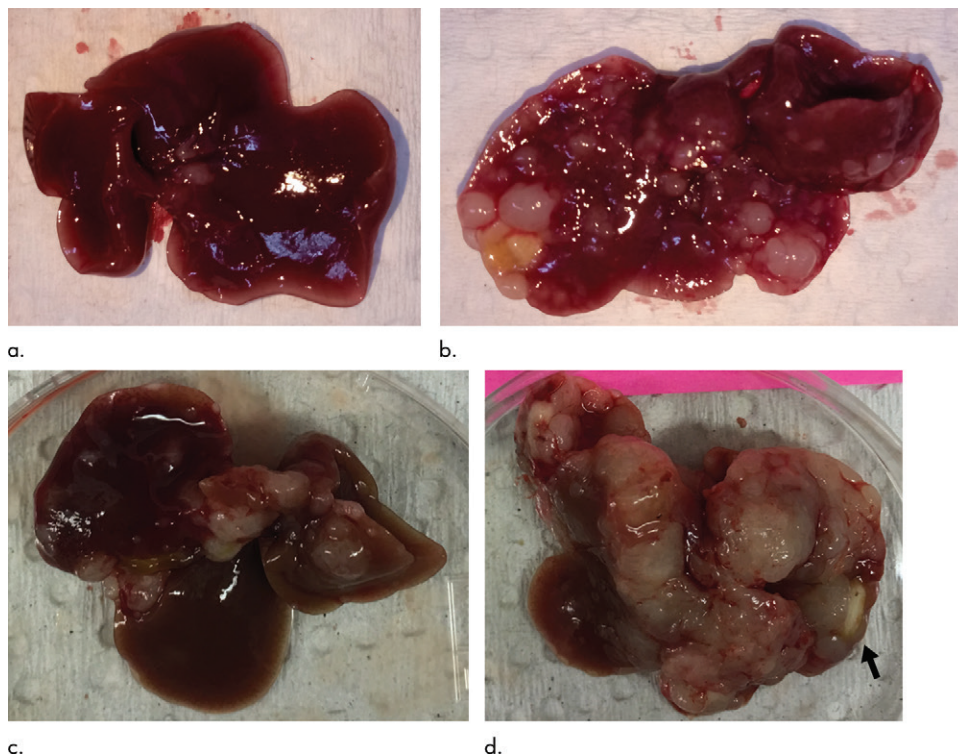
a.

b.

c.

d.

Figure 2: Intrahepatic metastatic tumor burden after radiofrequency ablation (RFA). Whole excised livers are presented as viewed from the ventral surface. At 14 days, the number of CT26 tumors in livers of **(a)** mice undergoing a sham procedure was significantly smaller than that in **(b)** mice that underwent RFA. Likewise, at 21 days, tumor number for **(c)** the sham group implanted with MC38 was overwhelmingly exceeded by that of **(d)** the RFA group. An ellipsoid white area (arrow in **d**) represents the visualized zone of residual radiofrequency-induced coagulation.

Table 1: Summary of Overall Tumor Load, Proliferative Index, and Neovascularization in Mice after Hepatic RFA or Sham Procedure

Parameter and Tumor Type	Sham Procedure	RFA	P Value
Tumor No.			
CT26	52 ± 44	103 ± 45	.009
MC38	39 ± 20	87 ± 51	.007
Tumor area ratio (%)			
CT26	39 ± 22	69 ± 20	.003
MC38	36 ± 20	62 ± 22	.007
Proliferative index (percentage Ki-67 positive per HPF)			
CT26	34 ± 8	69 ± 16	<.001
MC38	32 ± 17	64 ± 12	<.001
Neovascularization (no. CD34 positive per HPF)			
CT26	14 ± 5	63 ± 33	<.001
MC38	16 ± 6	29 ± 6	<.001

Note.—Data are means ± standard deviations. HPF = high-power field, RFA = radiofrequency ablation.

in the sham group ($P < .001$ for all comparisons) (Table 1; Figs 3, E1 [online]). Specifically, there was a greater percentage of Ki-67–positive cells (CT26: 69% per high-power field [HPF] ± 16 vs 34% per HPF ± 8; MC38: 64% per HPF ± 12 vs 32% per HPF ± 17 [Fig 3]); and more CD34-staining vessels in the tumor (CT26: 63 per HPF ± 33 vs 14 per HPF ± 5; MC38: 29 per HPF ± 6 vs 16 per HPF ± 6) (Fig E1 [online]) in the RFA group compared with the sham group.

Focal Hepatic RFA in Relationship to Tumor Cell Implantation and Metastases Development

Increases in intrahepatic tumor load, tumor proliferation, and angiogenesis were noted when injecting either CT26 or MC38 at both 1 day and 3 days after RFA (all P values $< .05$ for tumor growth, proliferation, and angiogenesis comparisons) (Fig 4). However, injection of tumor cells 7 days after RFA demonstrated no difference for tumor growth or any of the studied parameters ($P > .99$; Fig 4).

Relationship of Adjuvant Pharmacologic Targeting of c-Met and STAT3 and Tumorigenic Effect of RFA

The overall number of intrahepatic metastases after RFA was reduced with the addition of adjuvant PHA or S3I, compared with the RFA-alone arm ($P < .05$), to a number equivalent to the baseline, sham procedure arm ($P > .05$) (Tables 2, 3; Fig 5). Specifically, the number of tumors in the RFA plus PHA group was markedly less than that in the RFA-alone arm (CT26: 56 ± 28 for RFA + PHA vs 142 ± 28 for RFA alone, $P = .001$; MC38: 23 ± 18 RFA + PHA vs 139 ± 28 RFA alone, $P = .004$) and reduced to the baseline sham level (CT26: 93 ± 37, $P = .24$; MC38: 42 ± 14, $P = .24$). Tumor area ratio displayed a similar trend (CT26: RFA + PHA 33% ± 16 vs RFA alone 80% ± 9, $P < .001$; MC38: 16% ± 7 vs 90% ± 2, $P < .001$) (Table 2, Fig 5a). Similarly, a reduction in tumor cell proliferation was observed when administering RFA plus PHA. Specifically, percentages of Ki-67–positive cells receiving RFA plus PHA for both CT26 and MC38 (38% ± 10 and 22% ± 5, respectively) were lower than those observed with RFA alone (63% ±12 and 45% ± 12, respectively; $P < .001$ for both comparisons) and were equivalent to the baseline level of the sham procedure arm (38% ± 9, $P = .93$ and 21% ± 5, $P = .81$, respectively) (Table 2; Figs 5c, E2 [online]). Likewise,
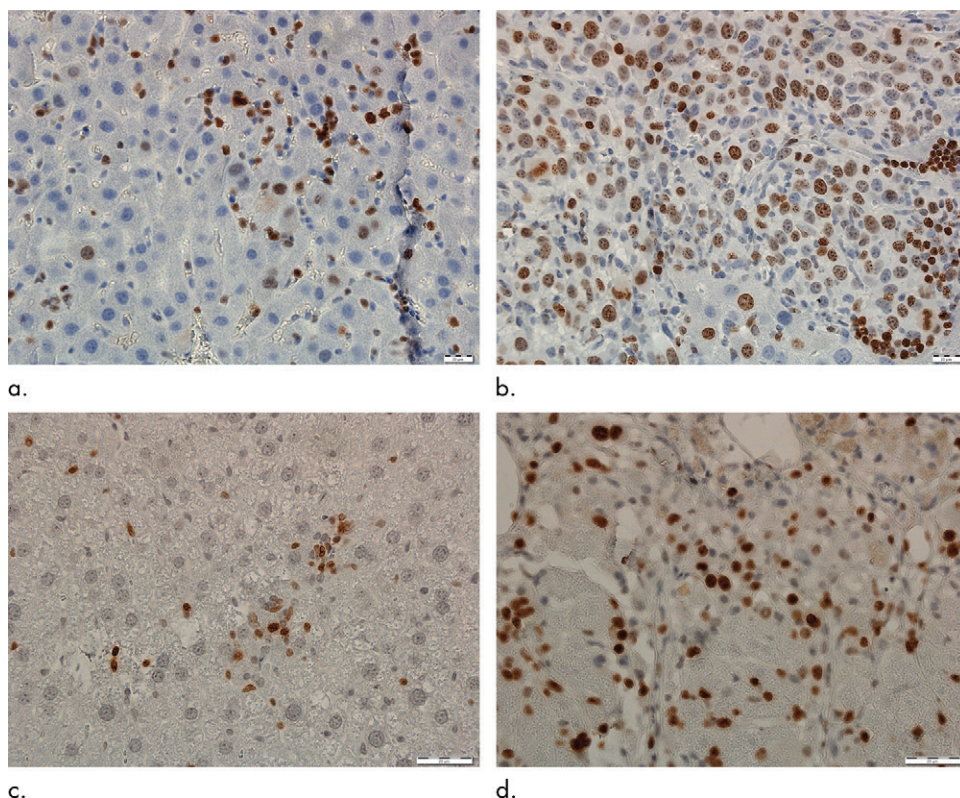
Figure 3: Photomicrographs show tumor proliferation induced by radiofrequency ablation (RFA) in mice. Brown dots = Ki-67–positive staining in the cellular nucleus (original magnification, ×40). Mice undergoing RFA developed more highly proliferative tumor cells than their littermates in the sham group. **(a)** Ki-67 in the sham group of Balb/C mice with CT26. **(b)** Ki-67 in the RFA group of CT26. **(c)** Ki-67 in the sham group of C57BL6 mice with MC38. **(d)** Ki-67 in the RFA group of C57BL6 mice with MC38.

the notion that RFA per se can promote oncogenic effects at the tumor initiation stage, and to already implanted yet microscopic tumors. Thus, promotion of intrahepatic metastatic growth is consistent with more robust engraftment of tumor cells, in addition to RFA's known effects of accelerating subcutaneous cancer deposits (15) and the facilitation of tumorigenicity to hepatocellular carcinoma (4,16). Our characterization of this RFA-induced tumor growth was accompanied by a significant synchronous increase in tumor proliferation (an increased percentage of Ki-67–positive cells, CT26: 69% per high-power field [HPF] $\pm$ 16 vs 34% per HPF $\pm$ 8; MC38: 64% per HPF $\pm$12 vs 32% per HPF $\pm$17; $P < .001$ for all comparisons) and neovascularization (CD34-positive cell count, CT26: n = 63 per HPF $\pm$ 33 vs 14 per HPF $\pm$ 5; MC38: 29 per HPF $\pm$ 6 vs 16 per HPF $\pm$ 6; $P < .001$ for all comparisons) in mice treated with ablation in comparison with those undergoing sham procedures. These data were consistent and reproducible in two different carcinoma cell lines in two strains of mice, suggesting that such tumor promotion after RFA may be representative and robust.

Defining the kinetics of these protumorigenic processes is necessary for designing rational future clinical treatment strategies to eliminate this effect. Thus, as a next step, the tumor transplantation was performed injecting cells 1 day to 7 days after ablation. Fortunately, we observed RFA tumorigenesis only over a relatively short temporal window. Increases in intrahepatic tumor burden, tumor proliferation, and angiogenesis were noted at both 1- and 3-day intervals after RFA/transplantation. However, transplantation of tumor cells 7 days after RFA demonstrated no statistical difference compared with the sham group for all indicators studied, suggesting that the effect of tumor promotion induced by RFA maintains a short-lived temporal window of less than 7 days.

In previous studies, hepatic RFA increased IL-6, HGF, and c-Met activity, leading to downstream VEGF-driven microvascular growth and proliferation (13,16,17). IL-6 levels in both the serum and periablational liver were markedly elevated by 6–12 hours after RFA (12,15). Likewise, the peak concentrations of HGF and VEGF occurred 72 hours after ablation in serum, periablational liver, and distant tumor (12,15). Thus, the window of maximum expression of these cytokines matches

a reduction in tumor vascularization also occurred within the group receiving RFA plus PHA (CD34-positive cells for CT26: 13 $\pm$ 3 and for MC38: 14 $\pm$ 5) compared with baseline levels (vs sham, $P > .72$ and vs RFA alone, $P < .001$ for both cell lines) (Table 2, Fig 5e). In similar fashion, the total tumor number, area ratio, proliferation, and microvascular density for RFA plus S3I was less than those in RFA ($P < .05$) and showed no difference compared with sham treatment ($P > .05$) (Table 3; Figs 5b, 5d, 5f, E3 [online]).

Discussion

We developed two rodent colorectal tumor models to study the effect of radiofrequency ablation (RFA) on intrahepatic metastatic growth from both CT26 and MC38 cells delivered by intrasplenic injection, thereby mimicking the influence of RFA on residual cancer cells diffused by seeding into the liver (21). We advance the understanding of this protumorigenic process by demonstrating that RFA significantly increased intrahepatic metastatic tumor numbers and volume (CT26: n = 103 $\pm$ 45 vs 52 $\pm$ 44, $P = .009$; MC38: 87 $\pm$ 51 vs 39 $\pm$ 20, $P = .007$; RFA vs sham, respectively) compared with sham procedures. By ablating visually normal liver tissue and observing increases in tumor load, we confirmed that the response to hyperthermic injury is indeed a fundamental factor of protumorigenic effects (19). Given the extensive increase in tumor observed only weeks after injection of individual cells, our data also support
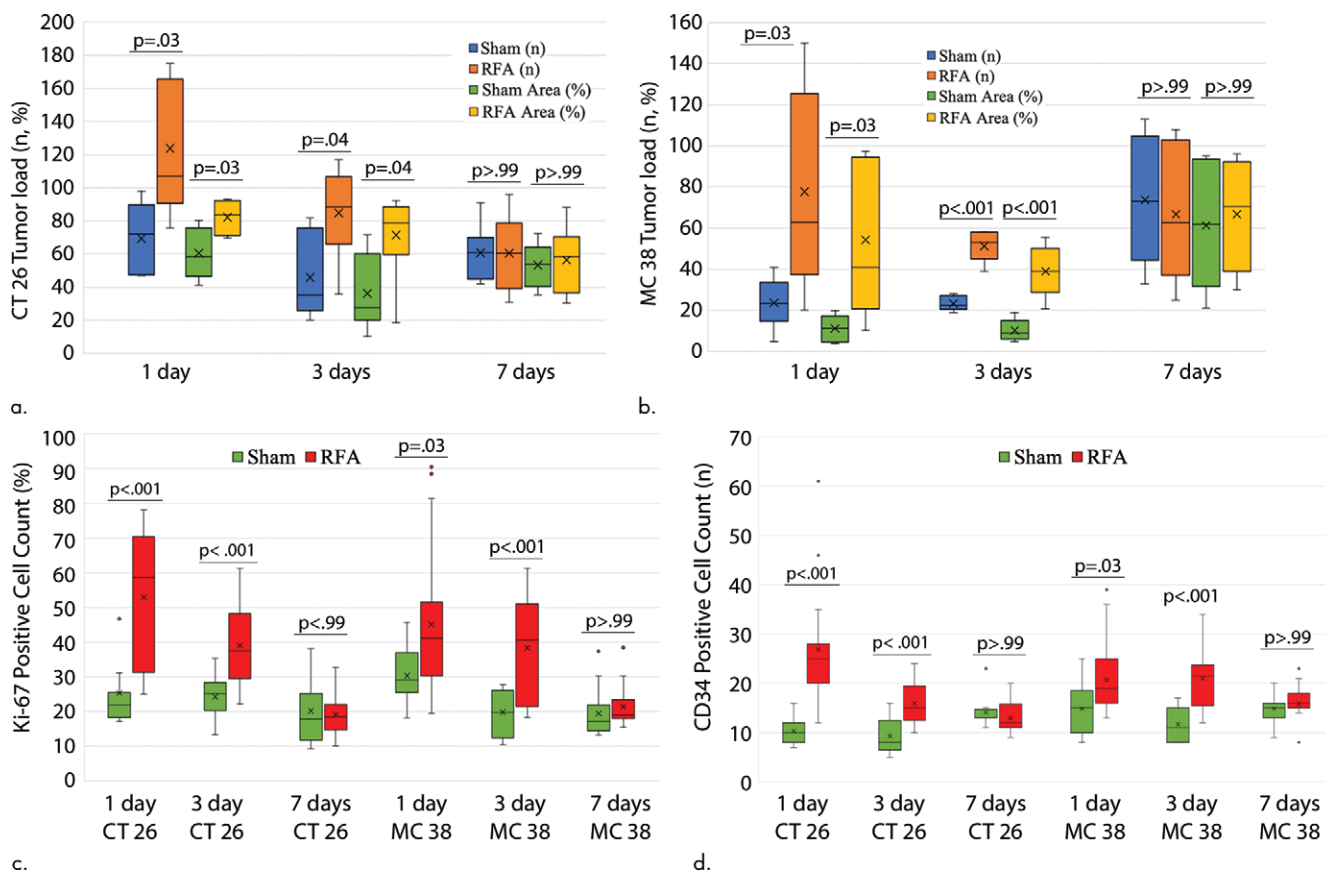
Figure 4: Graphs show comparison of metastatic load, proliferation, and neovascularization for tumor transplantation at various times after radiofrequency ablation (RFA). **(a)** The intrahepatic load of CT26 tumor in RFA was drastically greater than that in the sham group when CT26 cells were injected either 1 day or 3 days after RFA. **(b)** Likewise, intrahepatic load of MC38 tumor in RFA was greater than that of the sham group when cells were injected either 1 day or 3 days after RFA. **(c)** Cell proliferation of both CT26 and MC38 tumor in RFA was drastically increased over that in the sham group when tumor cells were transplanted either 1 day or 3 days after RFA, and **(d)** neovascularization in both tumors was drastically greater for RFA than that in the sham group when tumor cells were transplanted either 1 day or 3 days after RFA. However, transplantation of tumor cells 7 days after RFA resulted in no statistical difference for any of these parameters.

our findings for implanted metastases in which all indexes of tumor growth were most elevated 24 hours after ablation, remaining so for at least 3 days.

These kinetics are also consistent with the results of gene expression analysis (15). In one rodent study comparing hepatic RFA and sham procedures, the greatest number of differentially expressed genes (ie, 217) was observed at 24 hours, both in the periablational rim and the untreated liver lobe, with drastic, progressive declines in differentially expressed genes seen at 3 and 7 days. This included eight modulated biologic pathways identified at 24 hours after RFA, in which STAT3 was identified as a common mediator. Moreover, phosphorylated STAT3 expression was also increased in the periablational rim at 24 hours (15).

We further demonstrated that activated cytokinetic pathways can be successfully blocked by administering adjuvant drugs against key receptor targets, which contribute to metastatic growth stimulated by RFA. Here, a c-Met inhibitor successfully suppressed intrahepatic metastatic growth, (CT26: $n = 56 \pm 28$ for RFA + PHA vs 142 ± 28 for RFA alone, $P = .001$; MC38: 23 ± 18 for RFA + PHA vs 139 ± 28 for RFA alone, $P = .004$), with associated reduction in tumor cell proliferation and angiogenesis. Adjuvant PHA administered 2 hours before RFA resulted in the prevention of increased tumor growth and reduction to baseline

sham levels. PHA was likely acting in the periablational rim, where adjuvant PHA may block the HGF/c-Met–positive feedback loop to suppress periablational HGF levels. PHA may also have acted at tumors located in other lobes of the liver, where despite persistent high circulating levels of HGF, the RFA-induced growth stimulation was blocked (10,13,14,24,25).

Another signal inhibitor, STAT3 inhibitor (S3I), also successfully suppressed intrahepatic metastatic growth (CT26: $n = 16 \pm 8$ for RFA + S3I vs 81 ± 34 for RFA alone, $P = .005$; MC38: 29 ± 16 for RFA + S3I vs 68 ± 30 for RFA alone, $P = .02$). STAT3 is a member of the JAK-STAT signaling pathway, crucial for cancer initiation and progression (15,24,26,27). It is known to be responsible for tissue repair, inflammation, and increased angiogenic drive (25). STAT3 is a downstream signaling molecule activated by HGF and/or c-Met and can contribute to cell transformation induced by a diverse set of oncoproteins (13). Both PHA and S3I target specific mediators in a common pathway and were equally effective in our study. In particular, c-Met is closely linked to neoangiogenesis through stimulation of endothelial cells and VEGF production (28,29). STAT3 has been identified as a direct transcription activator of the VEGF gene, which may be activated by other non–c-Met pathways (30). Blocking STAT3 signaling can reduce tumor angiogenesis,

Table 2: Summary of Effect of c-Met Inhibition with PHA to Attenuate Post-RFA Tumorigenesis

Parameter and Tumor Type	Alone		Combined with PHA		P Value for RFA/PHA	
	Sham	RFA	Sham	RFA	vs Sham	vs RFA
Tumor no.						
CT26	93 ± 37	142 ± 28	66 ± 3	56 ± 28	.24	.001
MC38	42 ± 14	139 ± 28	40 ± 6	23 ± 18	.24	.004
Tumor area ratio (%)						
CT26	61 ± 13	80 ± 9	55 ± 14	33 ± 16	.07	<.001
MC38	55 ± 14	90 ± 2	36 ± 8	16 ± 7	.07	<.001
Proliferative index (percentage Ki-67 positive per HPF)						
CT26	38 ± 9	63 ± 12	37 ± 9	38 ± 10	.93	<.001
MC38	21 ± 5	45 ± 12	21 ± 5	22 ± 5	.81	<.001
Neovascularization (no. CD34 positive per HPF)						
CT26	14 ± 3	22 ± 3	13 ± 2	13 ± 3	.72	<.001
MC38	15 ± 4	26 ± 9	18 ± 6	14 ± 5	.81	<.001

Note.—Data are means ± standard deviations. HPF = high-power field, RFA = radiofrequency ablation.

Table 3: Summary of Effect of STAT3 Inhibition with S3I to Attenuate Post-RFA Tumorigenesis

Parameter and Tumor Type	Alone		Combined S3I		P Value for RFA/S3I	
	Sham	RFA	Sham	RFA	vs Sham	vs RFA
Tumor no.						
CT26	27 ± 12	81 ± 34	25 ± 13	16 ± 8	.76	.005
MC38	32 ± 17	68 ± 30	31 ± 13	29 ± 16	.98	.02
Tumor area ratio (%)						
CT26	31 ± 22	72 ± 18	23 ± 13	16 ± 7	.98	.003
MC38	25 ± 13	50 ± 22	28 ± 16	22 ± 15	.98	.03
Proliferative index (percentage Ki-67 positive per HPF)						
CT26	37 ± 7	60 ± 9	45 ± 9	39 ± 9	.98	<.001
MC38	38 ± 5	56 ± 10	35 ± 7	35 ± 8	.76	<.001
Neovascularization (no. CD34 positive per HPF)						
CT26	13 ± 2	20 ± 3	13 ± 3	12 ± 2	.98	<.001
MC38	12 ± 3	21 ± 5	13 ± 2	13 ± 2	.98	<.001

Note.—Data are means ± standard deviations. HPF = high-power field, RFA = radiofrequency ablation, S3I = STAT3 inhibitor, STAT3 = signal transducer and activator of transcription 3.

demonstrating that VEGF is downstream to STAT3 (15), which is consistent with our findings.

Our findings may be potentially relevant to metastases in other organs that respond to similar cytokines and proliferative factors that are released during the wound healing process after RFA. Accordingly, further study is needed to more extensively characterize the full scenario of conditions in which tumorigenic effects are to be encountered. Future work includes the following: *(a)* expanding the number of tumor types (including those with different genetic mutations or clinical risk scores) to determine which cell types are susceptible to protumorigenic effects–especially noting the fact that we studied only c-Met–positive tumors; *(b)* different relevant organ sites, where increased cytokinetic expression has been detected after RFA, particularly for kidney tumors and lung metastases, to determine effects in these organs; and *(c)* different sources of energy (eg, microwave, cryoablation, irreversible electroporation, high-intensity focused ultrasound, laser) and their dosimetry and techniques to determine the extent of variation among different commercially available ablation platforms (29). Moreover, a complementary future goal is to find tumor-specific characteristics and proper predictive biomarkers to maximize postablation clinical outcomes, because c-Met and STAT3 are not likely to be the only oncogenes or biomarkers associated with postablation tumorigenesis, as multiple additional pathways are likely to be involved in this process (31). This may permit personalized patient treatment by identifying which patients may benefit from adjuvant systemic therapy. Likewise, more full study of additional adjuvant medications, including optimal kinetics and doses, will need to be performed, including potential immunomodulators that induce counterbalancing systemic immunologic effects (32).
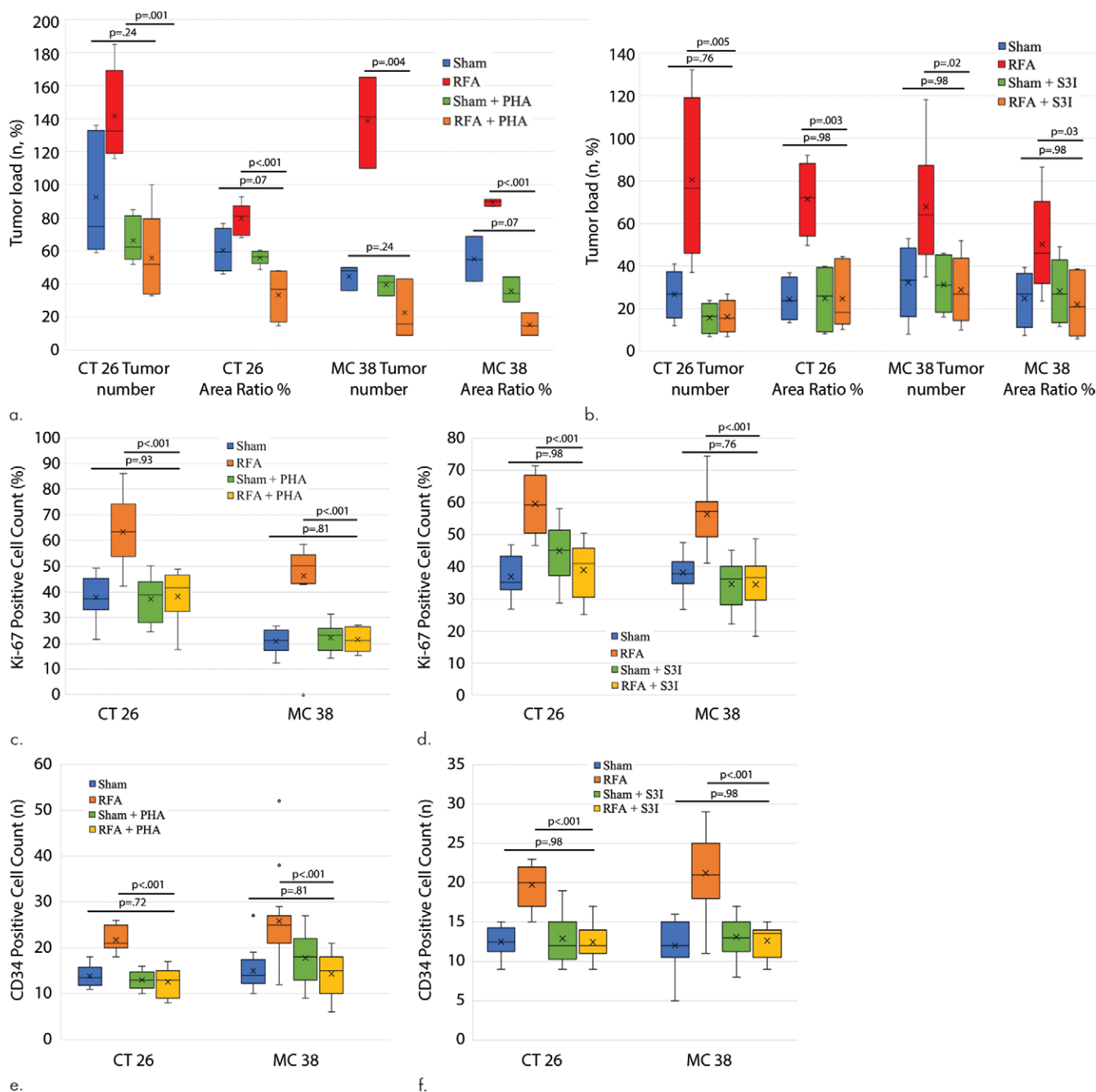
Figure 5: Graphs show that tumor load, proliferation, and microvascularization in mice undergoing radiofrequency ablation (RFA) are reduced after the administration of inhibitors of c-Met (ie, PHA) and signal transducer and activator of transcription 3 (S3I). **(a, b)** The overall tumor load of intrahepatic metastases after RFA declined to baseline with the addition of adjuvant PHA or S3I, compared with that in the group undergoing RFA alone ($P < .05$), with an overall number equivalent to that in the sham group ($P > .05$). **(c, d)** More proliferative tumor cells developed in mice undergoing RFA than in their littermates in the sham group ($P < .001$ for both CT26 and MC38), with proliferation reduced when RFA was combined with adjuvant PHA or S3I to an equivalent baseline level of the sham group ($P > .05$ for both tumor models). **(e, f)** Higher microvascular density was also noted within the tumor in the RFA group ($P < .001$ compared with sham for both tumor models), whereas lower microvascular density was observed when adjuvant PHA or S3I was administered after RFA and versus RFA alone ($P < .001$ for both cell lines), with no statistical difference from the sham procedure alone ($P > .05$ for both cell lines).

Potential limitations of our study included an experimental design performing splenic injections followed by splenectomy to maximize intrahepatic cellular implantation. We do acknowledge that such injection likely delivers greater amounts of tumor cells than present in clinical scenarios of circulating tumor cells or even a radiofrequency-induced tumor shower. Likewise, although tumor cells were injected at different time points after RFA to precisely determine at which time points accelerated tumor growth can be present, this too does not necessarily reflect the most likely clinical scenario. However, although we did not measure the precise number of cells in the circulation or portal vein at the time of injection, ultimately, all baseline sham groups had similar tumor burdens. Additionally, we note no lung or other distant metastases to suggest massive release of tumor into the circulation. Moreover,

splenectomy can potentially induce systemic hypoimmunity against tumors. Yet we note that all control mice were subjected to the same procedures and note adequate recovery of immune function following splenectomy (33,34).

In conclusion, although radiofrequency ablation (RFA) has been shown to be clinically useful, particularly for the treatment of intrahepatic tumors (2,6), ablation of a small volume of normal liver can stimulate intrahepatic metastatic implantation and growth, including tumor number and volume, tumorigenic proliferation, and neovascularization in mice. Our study is potentially highly clinically relevant to metastasis, particularly related to those types of cancer known to have circulating progenitor cancer cells that may implant following ablation. We demonstrate that this process is short lived, with a temporal window of less than 7 days after ablation. Moreover, our observations are consistent with prior work supporting the notion that the interleukin (IL)-6/IL-6R, hepatocyte growth factor/tyrosine-protein kinase Met, signal transducer and activator of transcription 3, vascular endothelial growth factor pathway is a major mechanism of the pro-oncogenic effect induced by hepatic RFA. Fortunately, we demonstrate that this phenomenon can be mitigated with individual receptor inhibitors, offering a potential strategy for reducing or eliminating this phenomenon in clinical practice with a short course of adjunctive therapy. Thus, further evaluation, including long-term survival and specific inhibition of pathways or growth factors by cutting-edge technologies such as CRISPR-CAS9, is likely warranted as a next step prior to clinical implementation.

References

1. Livraghi T, Goldberg SN, Lazzaroni S, et al. Hepatocellular carcinoma: radio-frequency ablation of medium and large lesions. Radiology 2000;214(3):761–768.
2. Solbiati L, Ahmed M, Cova L, Ierace T, Brioschi M, Goldberg SN. Small liver colorectal metastases treated with percutaneous radiofrequency ablation: local response rate and long-term survival with up to 10-year follow-up. Radiology 2012;265(3):958–968.
3. Ahmed M, Brace CL, Lee FT Jr, Goldberg SN. Principles of and advances in percutaneous ablation. Radiology 2011;258(2):351–369.
4. European Association for the Study of the Liver. EASL Clinical Practice Guidelines: Management of hepatocellular carcinoma. J Hepatol 2018;69(1):182–236 [Published correction appears in J Hepatol 2019;70(4):817.].
5. Gillams A, Goldberg N, Ahmed M, et al. Thermal ablation of colorectal liver metastases: a position paper by an international panel of ablation experts, The Interventional Oncology Sans Frontières meeting 2013. Eur Radiol 2015;25(12):3438–3454.
6. Ruers T, Van Coevorden F, Punt CJ, et al. Local Treatment of Unresectable Colorectal Liver Metastases: Results of a Randomized Phase II Trial. J Natl Cancer Inst 2017;109(9):djx015.
7. Park IJ, Kim HC, Yu CS, Kim PN, Won HJ, Kim JC. Radiofrequency ablation for metachronous liver metastasis from colorectal cancer after curative surgery. Ann Surg Oncol 2008;15(1):227–232.
8. Petre EN, Sofocleous C. Thermal Ablation in the Management of Colorectal Cancer Patients with Oligometastatic Liver Disease. Visc Med 2017;33(1):62–68.
9. Sotirchos VS, Petrovic LM, Gönen M, et al. Colorectal Cancer Liver Metastases: Biopsy of the Ablation Zone and Margins Can Be Used to Predict Oncologic Outcome. Radiology 2016;280(3):949–959.
10. Erinjeri JP, Thomas CT, Samoilia A, et al. Image-guided thermal ablation of tumors increases the plasma level of interleukin-6 and interleukin-10. J Vasc Interv Radiol 2013;24(8):1105–1112.
11. Hinz S, Tepel J, Röder C, Kalthoff H, Becker T. Profile of serum factors and disseminated tumor cells before and after radiofrequency ablation compared to resection of colorectal liver metastases - a pilot study. Anticancer Res 2015;35(5):2961–2967.
12. Rozenblum N, Zeira E, Bulvik B, et al. Radiofrequency Ablation: Inflammatory Changes in the Periablative Zone Can Induce Global Organ Effects, including Liver Regeneration. Radiology 2015;276(2):416–425.
13. Ahmed M, Kumar G, Moussa M, et al. Hepatic Radiofrequency Ablation-induced Stimulation of Distant Tumor Growth Is Suppressed by c-Met Inhibition. Radiology 2016;279(1):103–117.
14. Chang Q, Bournazou E, Sansone P, et al. The IL-6/JAK/Stat3 feed-forward loop drives tumorigenesis and metastasis. Neoplasia 2013;15(7):848–862.
15. Kumar G, Goldberg SN, Gourevitch S, et al. Targeting STAT3 to Suppress Systemic Pro-Oncogenic Effects from Hepatic Radiofrequency Ablation. Radiology 2018;286(2):524–536.
16. Rozenblum N, Zeira E, Scaiewicz V, et al. Oncogenesis: An "Off-Target" Effect of Radiofrequency Ablation. Radiology 2015;276(2):426–432.
17. Ahmed M, Kumar G, Navarro G, et al. Systemic siRNA Nanoparticle-Based Drugs Combined with Radiofrequency Ablation for Cancer Therapy. PLoS One 2015;10(7):e0128910.
18. Kumar G, Goldberg SN, Wang Y, et al. Hepatic radiofrequency ablation: markedly reduced systemic effects by modulating periablational inflammation via cyclooxygenase-2 inhibition. Eur Radiol 2017;27(3):1238–1247.
19. Nijkamp MW, Borren A, Govaert KM, et al. Radiofrequency ablation of colorectal liver metastases induces an inflammatory response in distant hepatic metastases but not in local accelerated outgrowth. J Surg Oncol 2010;101(7):551–556.
20. Schuld J, Richter S, Oberkircher LW, et al. Evidence for tumor cell spread during local hepatic ablation of colorectal liver metastases. J Surg Res 2012;178(1):268–279.
21. Massagué J, Obenauf AC. Metastatic colonization by circulating tumour cells. Nature 2016;529(7586):298–306.
22. Chudasama D, Rice A, Anikin V, Soppa G, Dalal P. Circulating Tumour Cells in Patients with Malignant Lung Tumors Undergoing Radio-frequency Ablation. Anticancer Res 2015;35(5):2823–2826.
23. Li Y, Huang N, Wang C, et al. Impact of liver tumor percutaneous radiofrequency ablation on circulating tumor cells. Oncol Lett 2018;16(3):2839–2850.
24. Goyal L, Muzumdar MD, Zhu AX. Targeting the HGF/c-MET pathway in hepatocellular carcinoma. Clin Cancer Res 2013;19(9):2310–2318.
25. García-Vilas JA, Medina MA. Updates on the hepatocyte growth factor/c-Met axis in hepatocellular carcinoma and its therapeutic implications. World J Gastroenterol 2018;24(33):3695–3708.
26. Jondal DE, Thompson SM, Butters KA, et al. Heat Stress and Hepatic Laser Thermal Ablation Induce Hepatocellular Carcinoma Growth: Role of PI3K/mTOR/AKT Signaling. Radiology 2018;288(3):730–738.
27. Rokavec M, Öner MG, Li H, et al. Corrigendum. IL-6R/STAT3/miR-34a feedback loop promotes EMT-mediated colorectal cancer invasion and metastasis. J Clin Invest 2015;125(3):1362.
28. Kitajima Y, Ide T, Ohtsuka T, Miyazaki K. Induction of hepatocyte growth factor activator gene expression under hypoxia activates the hepatocyte growth factor/c-Met system via hypoxia inducible factor-1 in pancreatic cancer. Cancer Sci 2008;99(7):1341–1347.
29. Velez E, Goldberg SN, Kumar G, et al. Hepatic Thermal Ablation: Effect of Device and Heating Parameters on Local Tissue Reactions and Distant Tumor Growth. Radiology 2016;281(3):782–792.
30. Yokogami K, Yamashita S, Takeshima H. Hypoxia-induced decreases in SOCS3 increase STAT3 activation and upregulate VEGF gene expression. Brain Tumor Pathol 2013;30(3):135–143.
31. Sofocleous CT, Garg S, Petrovic LM, et al. Ki-67 is a prognostic biomarker of survival after radiofrequency ablation of liver malignancies. Ann Surg Oncol 2012;19(13):4262–4269.
32. Erinjeri JP, Fine GC, Adema GJ, et al. Immunotherapy and the Interventional Oncologist: Challenges and Opportunities-A Society of Interventional Oncology White Paper. Radiology 2019;292(1):25–34.
33. Rosman CWK, Broens PMA, Trzpis M, Tamminga RYJ. A long-term follow-up study of subtotal splenectomy in children with hereditary spherocytosis. Pediatr Blood Cancer 2017;64(10):e26592.
34. Wu Z, Zhou J, Pankaj P, Peng B. Laparoscopic and open splenectomy for splenomegaly secondary to liver cirrhosis: an evaluation of immunity. Surg Endosc 2012;26(12):3557–3564.